nature physics

ARTICLES

https://doi.org/10.1038/s41567-018-0414-3

Quantum error correction and universal gate set operation on a binomial bosonic logical qubit

L. Hu[1,5], Y. Ma[1,5], W. Cai[1], X. Mu[1], Y. Xu[1], W. Wang[1], Y. Wu[2], H. Wang[1], Y. P. Song[1], C.-L. Zou[3*], S. M. Girvin[4], L-M. Duan[1,2] and L. Sun[1*]

Logical qubit encoding and quantum error correction (QEC) protocols have been experimentally demonstrated in various physical systems with multiple physical qubits, generally without reaching the break-even point, at which the lifetime of the quantum information exceeds that of the single best physical qubit within the logical qubit. Logical operations are challenging, owing to the necessary non-local operations at the physical level, making bosonic logical qubits that rely on higher Fock states of a single oscillator attractive, given their hardware efficiency. QEC that reaches the break-even point and single logical-qubit operations have been demonstrated using the bosonic cat code. Here, we experimentally demonstrate repetitive QEC approaching the break-even point of a single logical qubit encoded in a hybrid system consisting of a superconducting circuit and a bosonic cavity using a binomial bosonic code. This is achieved while simultaneously maintaining full control of the single logical qubit, including encoding, decoding and a high-fidelity universal quantum gate set with 97% average process fidelity. The corrected logical qubit has a lifetime 2.8 times longer than that of its uncorrected counterpart. We also perform a Ramsey experiment on the corrected logical qubit, reporting coherence twice as long as for the uncorrected case.

Quantum states are fragile and can easily be destroyed by their inevitable coupling to the uncontrolled environment, which presents a major obstacle to quantum computation[1]. A practical quantum computer capable of large circuit depth ultimately calls for operations on logical qubits protected by quantum error correction (QEC)[2–5] against unwanted errors. Realization of a logical qubit with a longer coherence time than its individual physical components is considered to be one of the most challenging goals for current quantum information processing[6]. For QEC, fragile quantum information needs first to be redundantly encoded in a logical subspace of a larger Hilbert space[4]. Error syndromes that can distinguish the code space from the orthogonal error subspaces need to be monitored repetitively without perturbing the encoded information. Using quantum non-demolition (QND) syndrome measurements, unitary recovery gates are adaptively applied to restore the original encoded information. QEC and realization of universal unitary manipulations of the logical qubit within the code space are necessary steps towards a practical quantum computer. The next stage is to demonstrate gate operations on the logical qubit under continuous QEC protection.

In standard logical qubit schemes based on multiple physical qubits[7–17], QEC and logical operations are difficult to achieve because the number of distinct error channels increases with the number of qubits, and non-local gates on a collection of physical qubits are required. A different encoding architecture based on a single bosonic oscillator has been proposed, using (for example) the Gottesman–Kitaev–Preskill codes[18] and the cat codes[19,20], and has attracted interest[21–30]. Taking advantage of the infinite-dimensional Hilbert space of a harmonic oscillator, quantum information can be encoded with a single degree of freedom. Most importantly, photon loss remains the dominant error channel, so there is still only one error syndrome that needs to be monitored. In addition, universal operations on the oscillator can be realized by dispersively coupling to a single ancilla transmon qubit, which allows fast and high-fidelity operations[31]. As a result, the requirements for hardware are greatly reduced[19,20]. For bosonic codes the break-even point is defined relative to the Fock $\{|0\rangle, |1\rangle\}$ encoding, since this non-correctable code has the lowest possible photon number and is thus the analogue of a single physical qubit. QEC protection exceeding the break-even point for quantum memory has been demonstrated with a cat-code encoding[24] and, separately, gate operations on such logical qubits have been demonstrated without any QEC protection[26].

In addition to the above advantages, the recently introduced binomial codes[32] have the advantage that the mean photon numbers (and for higher-order binomial codes, several moments of the photon number) are exactly equal, and furthermore admit an explicit unitary operation for repumping photons into the photonic mode. This contrasts with the originally proposed cat code[19,20], which suffers code deformations at small amplitudes owing to different mean photon numbers of the code words[33]. See Supplementary Information for further discussion of this point.

Binomial codes can exactly correct errors that are polynomial up to a specified order in photon creation and annihilation operators, including amplitude damping, dephasing and displacement noise, and thus provide significant improvement provided that the higher-order photon loss probabilities are sufficiently small. In addition, for a given mean photon number the required dimension of Fock space for a binomial code is smaller than that for a cat code, meaning that gate operations on the binomial logical qubit in principle should have higher fidelities owing to a smaller influence from Kerr effects. Recently, a controlled-NOT gate on a target qubit based on the lowest-order binomial code without QEC protection has been realized[28]. Here, we also choose the lowest-order binomial code that can protect against a single-photon loss error,

[1]Center for Quantum Information, Institute for Interdisciplinary Information Sciences, Tsinghua University, Beijing, China. [2]Department of Physics, University of Michigan, Ann Arbor, MI, USA. [3]Key Laboratory of Quantum Information, CAS, University of Science and Technology of China, Hefei, China. [4]Departments of Applied Physics and Physics, Yale University, New Haven, CT, USA. [5]These authors contributed equally: L. Hu, Y. Ma.
*e-mail: clzou321@ustc.edu.cn; luyansun@tsinghua.edu.cn

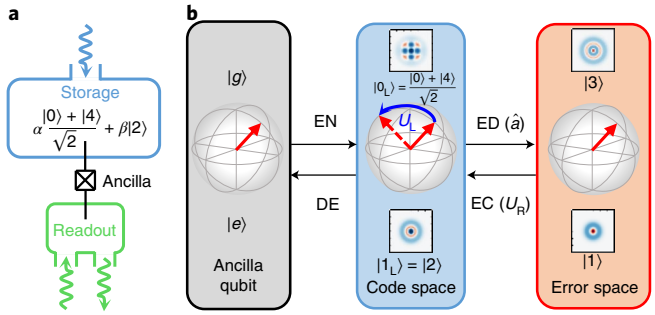

Fig. 1 | Schematic of the experiments on binomial quantum code. **a**, The experimental device consists of a storage cavity as an oscillator for logical quantum state encoding, an ancillary transmon qubit facilitating all quantum operations, and a readout cavity for the ancilla measurement. The quantum states are encoded in the oscillator with the binomial code basis states $|0_L\rangle = (|0\rangle + |4\rangle)/\sqrt{2}$ and $|1_L\rangle = |2\rangle$. **b**, Operations on a single logical qubit. The quantum state of the ancilla qubit $\{|g\rangle, |e\rangle\}$ can be encoded (EN) to and decoded (DE) from the code space of the oscillator. A single-photon loss changes the code space with even parity to the error space $\{|3\rangle, |1\rangle\}$ with odd parity. A high-fidelity and QND parity measurement can detect this error event, while leaving encoded quantum information untouched. Once a loss error is detected (ED), a unitary error correction (EC) recovery gate U_R can convert the error space back to the original code space. If no parity jump is detected, the deterministic evolution of the code word can be corrected by another unitary recovery gate (not shown), completing a closed-loop QEC on the logical qubit. With the assistance of the ancilla, high-fidelity gate operations U_L on the logic qubit can also be implemented within the code space.

and demonstrate full control of a single bosonic logical qubit with a repetitive QEC and a high-fidelity universal gate set (97.0% average process fidelity). The corrected logical qubit exhibited a lifetime 2.8 times longer than that of the uncorrected binomial logical qubit, and approaches the break-even point. The complete logical qubit operations demonstrated here could be the foundation for developing fault-tolerant quantum computing[6,34] and one-way quantum repeaters[33]. Additionally, we perform a Ramsey experiment on the QEC protected logical qubit that shows a coherence two times longer than that of the uncorrected logical qubit, paving the way towards QEC-enhanced quantum metrology[35]. Our demonstration could also be generalized to superconducting systems hybridized with other bosonic excitations[36].

The bosonic logical qubit experiment is implemented in a circuit quantum electrodynamics architecture[37,38] with a transmon qubit dispersively coupled to two three-dimensional cavities[21,22,24,38,39], illustrated schematically in Fig. 1a. The ancilla qubit has an energy relaxation time $T_1 = 30\,\mu s$ and a pure dephasing time $T_\phi = 120\,\mu s$. The storage cavity serving as an oscillator (henceforth referred as the 'oscillator') for encoding logical quantum states has a single-photon lifetime $\tau_s = 143\,\mu s$ (corresponding to $\kappa_s/2\pi = 1.1\,kHz$) and a Ramsey phase coherence time 252 μs. Utilizing the large Hilbert space of the harmonic oscillator, we construct the binomial code by superposing Fock states with binomial coefficients[32]. In our experiment, we choose the lowest-order binomial code with the code words:

$$|0_L\rangle = (|0\rangle + |4\rangle)/\sqrt{2} \quad (1)$$

$$|1_L\rangle = |2\rangle \quad (2)$$

as shown in Fig. 1b. Both basis states have the same average photon number of two, as required by the QEC criteria[1]. This code can protect quantum information from single-photon loss errors, which is the dominant error channel for the microwave oscillator. A single-photon loss sends the logical states from the code space with even parity to an error space with odd parity, that is $\hat{a}\,|0_L\rangle = \sqrt{2}\,|3\rangle$ and $\hat{a}\,|1_L\rangle = \sqrt{2}\,|1\rangle$, where $\hat{a}$ is the photon annihilation operator of the oscillator.

A complete set of operations on the bosonic logical qubit is illustrated in Fig. 1b. Besides serving as an ancilla for the error syndrome detection of the logical qubit, the transmon qubit provides the necessary non-linearity for implementing the quantum encoding, decoding and error-correcting recovery operation (U_R), as well as the universal single logical qubit operations in the binomial code space (logical gates U_L). Through a sequence of control pulses on the system, all these operations on the logical qubit are realized, based on the dispersive interaction between the ancilla and the oscillator[24,40]

$$H_{int} = -\chi_{qs}\hat{a}^\dagger\hat{a}\,|e\rangle\langle e| - \frac{K}{2}\hat{a}^{\dagger 2}\hat{a}^2 \quad (3)$$

where $|e\rangle$ is the excited state of the ancilla qubit ($|g\rangle$ is the ground state), $\chi_{qs}/2\pi = 1.90\,MHz$ is the dispersive interaction strength and $K/2\pi = 4.2\,kHz$ is the self-Kerr coefficient of the oscillator. The control pulses are synchronized and generated by field programmable gate arrays with home-made logic, and allow for fast real-time feedback control of the logical qubit (see Supplementary Information for the experimental apparatus). The pulse shapes are numerically optimized using the gradient ascent pulse engineering (GRAPE) method[41,42], based on carefully calibrated experimental parameters.

First, we demonstrate the encoding and decoding process, where quantum information is transferred between the ancilla qubit $\{|g\rangle, |e\rangle\}$ and the binomial code space $\{|0_L\rangle, |1_L\rangle\}$ of the oscillator. Process tomography[1] is used to benchmark our encoding and decoding performance, and the fidelity is defined as $F_\chi = \mathrm{tr}(\chi_M\chi_I)$, with $\chi_M(\chi_I)$ being the derived 4×4 process matrix for experimental (ideal) operation (see Methods). Figure 2b shows the χ_M for a sequential encoding and decoding process and indicates a fidelity of 93.1%.

The quantum information in the binomial code space can be protected from a single-photon loss by the QEC process (including both error detection and correction). A photon number parity measurement can distinguish the code and error spaces (Fig. 1b) without perturbing the encoded information[22], and thus serves as the error syndrome for error detection. Once a parity change is detected, the state in the error space can be converted back to the original code space by a unitary recovery gate U_R. As opposed to the cat code, where corrections can be performed at the end of error-syndrome tracking[24], the photon loss error in our experiment needs to be corrected immediately, because this particular binomial code does not tolerate two or more photon losses. Repeated such processes can therefore protect the information stored in the logical qubit. As usual, a trade-off needs to be considered between more frequent parity measurement to avoid missing photon loss errors and finite detection and recovery fidelities causing extra information loss.

The experimental protocol for repetitive QEC is shown in Fig. 2a, where a two-layer QEC procedure is adapted to balance the operation errors, no-parity-jump back-action errors and photon-loss errors. The top-layer QEC consists of several bottom-layer QEC steps, and (since double-photon loss would be fatal) each step corrects photon-loss error but tolerates the back action from the detection of no parity jump until the last step. Therefore, the top-layer QEC recovers the quantum information in the code space and is repeated many times, while the bottom-layer QEC conserves parity in a deformed code space. The current experiment consists of two bottom-layer QEC steps with an optimal waiting time $t_w = 17.9\,\mu s$ (see Fig. 3b). The number of bottom-layer QEC steps is chosen as

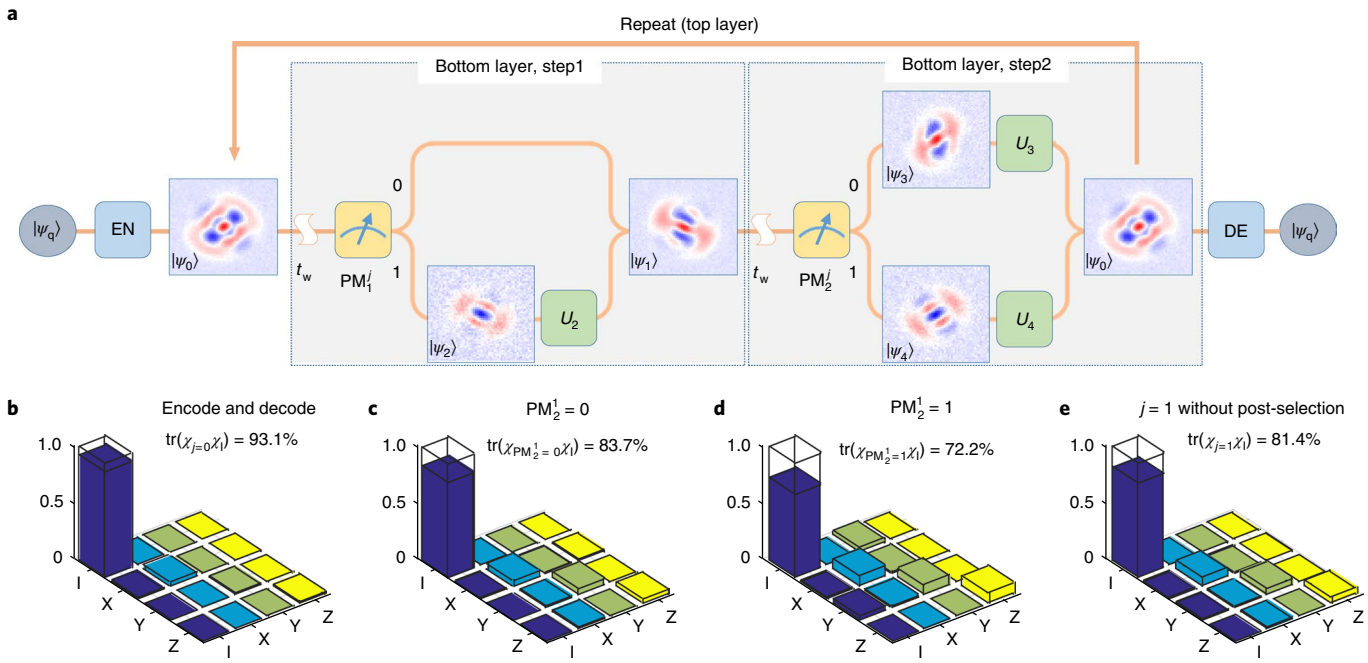

Fig. 2 | Protocol of the repetitive QEC and process tomography. a, The experimental procedure. The experiment begins with encoding an arbitrary superposition state $|\psi_q\rangle = \alpha\ |g\rangle + \beta\ |e\rangle$ of the ancilla qubit onto the oscillator state $|\psi_0\rangle = \alpha(|0\rangle + |4\rangle)/\sqrt{2} + \beta\ |2\rangle$ (process EN). After a waiting time $t_w \approx 17.9\,\mu s$, a parity measurement is performed. $PM_1^j = 0$ (the first parity measurement of the jth round) indicates that no photon-loss error occurs (two or more photon-loss errors cannot be distinguished but have a small probability), and the state of the oscillator undergoes a deterministic evolution to a deformed code space as $|\psi_1\rangle = \alpha(\cos\theta_1\ |0\rangle + \sin\theta_1 e^{i\varphi_4}\ |4\rangle)/\sqrt{2} + \beta e^{i\varphi_2}\ |2\rangle$, and no correction action is applied. $PM_1^j = 1$ indicates that one photon-loss error occurs, and the oscillator state becomes $|\psi_2\rangle = \alpha e^{i\varphi_3}\ |3\rangle + \beta\ |1\rangle$. A π pulse is first applied to flip the ancilla qubit to the $|g\rangle$ state to minimize the detrimental effect from the ancilla qubit decoherence, and then a unitary recovery gate U_2 is applied immediately to convert $|\psi_2\rangle$ to $|\psi_1\rangle$. Note that after another waiting time t_w, a second parity measurement is performed. Similarly, $PM_2^j = 0$ or 1 indicates that no or one photon loss occurs, and the oscillator state becomes $|\psi_3\rangle = \alpha(\cos\theta_2\ |0\rangle + \sin\theta_2 e^{i\varphi_4'}\ |4\rangle)/\sqrt{2} + \beta e^{i\varphi_2'}\ |2\rangle$ and $|\psi_4\rangle = \alpha e^{i\varphi_3'}\ |3\rangle + \beta\ |1\rangle$, respectively. Unitary gates U_3 and U_4 are then applied correspondingly to restore the original state $|\psi_0\rangle$. This error correction process is repeated 1–19 times followed by a decoding process (DE) to the ancilla qubit. $|\psi_{0-4}\rangle$ are all measured Wigner functions for $\alpha = 1/\sqrt{2}$ and $\beta = -i/\sqrt{2}$. **b**–**e**, χ matrices of the process tomography, showing encoding followed immediately by the decoding process (**b**), one round of error correction for $PM_2^1 = 0$ (with probability 79.3%) and $PM_2^1 = 1$ (with probability 20.7%), respectively (**c** and **d**), and one round of correction without post-selecting $PM_2^1 = 0$ or 1 (**e**). I, X, Y and Z are the Pauli basis. Here, only the real parts are shown while the imaginary parts are nearly zero.

a compromise between tolerating more back action from the detection of no parity jump and fewer adaptive gate operations (see Supplementary Information). The outcome of first error detection PM = 0 indicates that no photon-loss error occurs and the state of the oscillator undergoes an evolution from $|\psi_0\rangle = \alpha\ |0_L\rangle + \beta\ |1_L\rangle$ to $|\psi_1\rangle = \alpha\ |0_L'\rangle + \beta\ |1_L'\rangle$, with a deformation of code space basis states $|0_L'\rangle = \cos\theta_1\ |0\rangle + \sin\theta_1 e^{i\varphi_4}\ |4\rangle$ and $|1_L'\rangle = e^{i\varphi_2}\ |2\rangle$. We note that the above unitary evolution is only an approximation to the non-unitary back action associated with the no-parity-jump evolution $e^{-(\kappa_s/2)\hat{a}^\dagger\hat{a}t}$ valid to first order in $\kappa_s t_w$[32]. It is also worth noting that no detected parity change cannot rule out the possibility of having two-photon losses (about 2.1%), which causes complete quantum information loss. For PM = 1, one photon-loss error occurs (the probability of having a three-photon loss of about 0.14% can be neglected), and the oscillator state becomes $|\psi_2\rangle = \alpha e^{i\varphi_3}\ |3\rangle + \beta\ |1\rangle$ and a unitary recovery gate U_2 has to be applied immediately to convert $|\psi_2\rangle$ to $|\psi_1\rangle$ in the deformed code space. After an additional waiting time t_w, another error detection is performed for the second bottom-layer QEC step. Similarly, PM = 0 and 1 indicate a further deformation of code space to $|\psi_3\rangle$ and a jump to error space with $|\psi_4\rangle = \alpha e^{i\varphi_3'}\ |3\rangle + \beta\ |1\rangle$, respectively. Then unitary gates U_3 and U_4 are applied correspondingly to restore the original state $|\psi_0\rangle$, completing one round of top-layer error correction. In Fig. 2c–e, the process matrices are presented for the process after the second error detection in the first round of top-layer QEC, showing a good fidelity of 81.4%.

Figure 3a shows the process fidelity $F_\chi(t)$ with the repetitive QEC (green) decaying exponentially as a function of time, where the two-layer error correction process is repeated $j = 1$–19 times. For comparison, the process fidelities of the uncorrected binomial quantum code (red), the uncorrected transmon qubit (black), and the uncorrected Fock state $\{|0\rangle, |1\rangle\}$ encoding of the oscillator (blue) are also plotted. All curves are fitted using $F_\chi(t) = 0.25 + Ae^{-t/\tau}$, where τ is the lifetime. τ of the corrected binomial code is 5.3 times longer than the uncorrected transmon qubit, 2.8 times longer than the uncorrected binomial code, and only 8% or less lower than the uncorrected Fock encoding that defines the break-even point for the QEC[23]. These results demonstrate that the experimental system and scheme are robust and can indeed protect the encoded bosonic code from the photon loss error.

The experiment with the two-layer QEC procedure is limited mainly by the decoherence of the ancilla qubit, which induces imperfections and deserves further investigation. Since the ancilla facilitates both error detection and gate operations, the ancilla decoherence induces errors for these processes and prevents more frequent QEC. On the other hand, with a larger interval between QECs, there is a higher probability of having undetectable two-photon losses and a larger dephasing effect induced by photon losses owing to the non-commutativity of the annihilation operation $\hat{a}$ and the self-Kerr term $\frac{K}{2}\hat{a}^{\dagger 2}\hat{a}^2$. To illustrate this trade-off, Fig. 3b shows the numerically predicted decay time as a function of the tracking interval per two error detections following the protocol in Fig. 2a

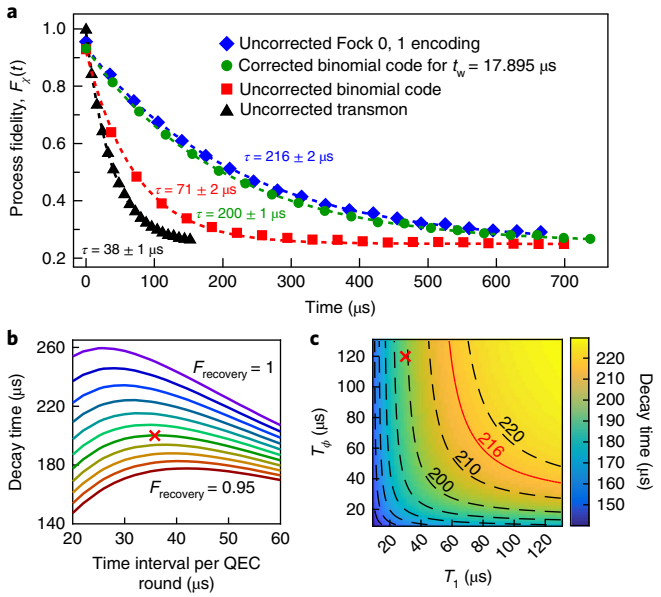

Fig. 3 | QEC performance. a, The green curve shows process fidelity $F_\chi(t)$ with the repetitive QEC decaying exponentially as a function of time. Each point is obtained by averaging 40,000 measurements and the error bars are smaller than marker sizes. For comparison, the process fidelity decay curves of the uncorrected binomial quantum code (red), the uncorrected transmon qubit (black), and the uncorrected Fock state $\{|0\rangle, |1\rangle\}$ encoding (blue) are also plotted. All curves are fitted using $F_\chi(t) = 0.25 + Ae^{-t/\tau}$ (dotted lines). **b**, Theoretically expected process fidelity decay time for the protocol in Fig. 2a with the measured parameters but with different recovery gate fidelities (the coloured lines correspond to fidelities from 0.95 to 1 with a step of 0.005). The cross indicates our experimental result, implying a recovery gate fidelity of about 97.0%. **c**, Expected process fidelity decay time as a function of T_1 and T_ϕ. Dashed lines represent isolines from 150 μs to 220 μs with a step of 10 μs. The cross indicates our experimental result. The red line represents the break-even condition. To extend the logical qubit lifetime beyond that of the Fock state $\{|0\rangle, |1\rangle\}$ encoding, T_1 needs to be doubled while T_ϕ remains the same.

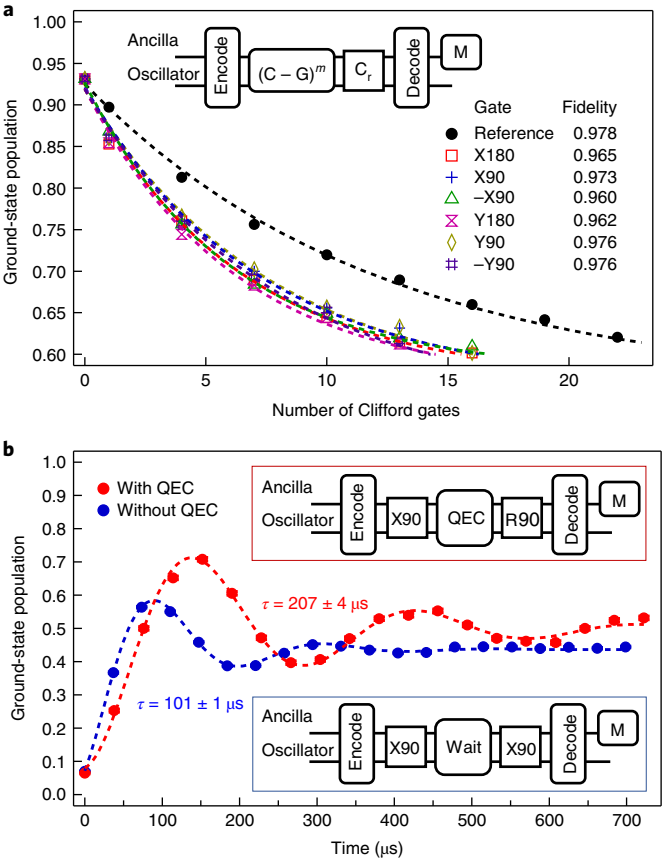

Fig. 4 | Gate operations on the logical qubit and Ramsey interferometry on the QEC-protected logical qubit. a, Randomized benchmarking is used to quantify the gate performance on the logical qubit, with the protocol shown in the inset. All experiments start with an encoding and end with a decoding followed by an ancilla qubit measurement (M). The reference curve is measured after applying sequences of m random Clifford gates (C), while the other curves are realized after applying sequences that interleave the corresponding gate G (±X90, ±Y90, X180, Y180, that is, $\pm\pi/2$ rotation along the x or y axis, and π rotation along the x or y axis, respectively) with m random Clifford gates. Each sequence is followed by a recovery Clifford gate (C_r) at the end just before the final measurement. The number of random sequences for each length m in our experiment is $k = 100$ and each random sequence is repeated over 5,000 times. All curves are fitted by $F_{RB} = Ap^m + B$ with different sequence decay p. The reference decay indicates the average error of the single-qubit gates, while the ratio of the interleaved and reference decay gives the specific gate fidelity. The averaged single-qubit gate error $r_{gate} \approx 0.031$. **b**, Ramsey interferometry of logical qubit, with insets showing the experimental sequences. The Ramsey oscillation on the QEC-protected logical qubit (red) gives a coherence time twice as long as that without QEC protection (blue), demonstrating a real gain of the coherence from QEC. For the process without QEC, the intervals between gates are chosen such that the Kerr rotations of $|4\rangle$ are integer multiples of 2π. The rotation axis of the second $\pi/2$ gate is fixed and the oscillation comes from the Kerr rotation of $|2\rangle$. The population converges to a value slightly lower than 0.5, which comes from the leakage of the encoded state out of the computational space during the long process without protection. For the QEC-protected case, the rotation axis of the second $\pi/2$ gate (R90) varies in the x–y plane with an interval of $\pi/4$.

(see Supplementary Information). It predicts a shorter optimal t_w and a longer decay time for a higher recovery gate fidelity. Our experimental result is indicated by the cross, implying a recovery gate fidelity of about 97.0% that is mainly limited by the ancilla qubit decoherence during the recovery gates. To extend the logical qubit lifetime beyond that of the Fock state $\{|0\rangle, |1\rangle\}$ encoding, either a better strategy with at least four bottom-layer QEC steps needs to be implemented with current qubit coherence (although this requires more adaptive gate operations; see Supplementary Information), or the coherence time of the ancilla qubit needs to be improved. As depicted in Fig. 3c, this goal can be achieved if we can double T_1 while keeping the same T_ϕ. By comparison, a cat code does not have this recovery gate error issue, and instead only requires tracking of the number of errors and a correction at the end of the whole QEC process[24] (provided that the cat-state amplitudes remain large enough). If the recovery gate itself is perfect and we have only detection errors, we can in principle achieve a decay time after QEC of over 260 μs, more than 20% longer than for the Fock state $\{|0\rangle, |1\rangle\}$ encoding.

To fully exploit the binomial encoding for future quantum information processing, gate operations on the logical qubits are indispensable. Thanks to the single bosonic oscillator encoding, we are able to implement the logical qubit gates by universal control of the state of the oscillator, instead of encoding/decoding to the ancilla qubit. We performed a randomized benchmarking experiment[43–46] to determine the fidelity of the Clifford gates on the logical qubit. Figure 4a shows the results with an average gate error $r_{gate} \approx 0.031$. These gate fidelities could be improved further by a more careful

calibration of the GRAPE pulses. Since the T gate does not belong to the Clifford group, in our experiment, we instead performed repeated gates to extract its gate fidelity, of about 98.7% (data shown in the Supplementary Information). We note that recently it has been proposed that the T gate can also be characterized by randomized benchmarking[47–49].

With QEC and high-fidelity universal operation of the logical qubit in hand, we demonstrate a Ramsey experiment on the QEC-protected logical qubit that indeed shows longer coherence. The insets to Figure 4b show the experimental sequences for the logical qubit Ramsey experiments with and without QEC, and both experiments also combine an encoding and decoding process. The results are fitted with an exponentially damped sinusoidal function. The Ramsey experiment performed on the logical qubit without QEC gives a coherence time of 101 μs. The interference fringes against the evolution time correspond to a Kerr-nonlinearity-induced phase change of the logical qubit. It is worth noting that the self-Kerr does not cause errors in the lowest-order binomial code in the absence of cavity photon decay. A particular frame can be chosen to match the rotation of $|4\rangle$ relative to $|0\rangle$ so that $|0\rangle$ and $|4\rangle$ are degenerate, while $|2\rangle$ has a slightly different frequency. However, the resulting phase rotation of the logical qubit is purely deterministic and so there is no decoherence associated with the self-Kerr effect. This is true even if the higher-order corrections to Kerr nonlinearity are taken into account, which is a useful feature of the lowest-order binomial code.

For comparison, the experiment on the QEC-protected logical qubit gives a coherence time of 207 μs, twice as long as without QEC protection, demonstrating a real gain in coherence from QEC. The Ramsey oscillation in this QEC-protected case comes from the variable rotation axis of the second $\pi/2$ gate. Since Ramsey interferometry is widely used for precision measurements, our results represent an important advance towards QEC-enhanced metrology based on logical qubits.

In addition to the real-time repetitive QEC and universal gate set on a bosonic logical qubit demonstrated in this work, two-logical-qubit gates still remain to be demonstrated for universal quantum computation. Our work provides a starting point for future work: to realize a logical qudit with binomial code, to generalize the tools realized in this work to multiple oscillators (logical qubits) and to realize fault-tolerant error detection and correction, as well as logical gates. Current experimental techniques could realize more logical qubits by integrating more cavities or modes in a compact three-dimensional structure[50]. Our results motivate further investigation of superconducting quantum processors, paving the way towards fault-tolerant implementation of QEC and gates based on bosonic encodings[6,34]. The quantum bosonic code demonstrated here can also be directly applied to phonon[51] and magnon[52] excitations by hybridizing with superconducting circuits. In addition, a similar architecture could be realized in the neutral atom[53] and trapped-ion[54] systems, in which the atomic motion provides a bosonic mode with long coherence times while the internal atomic energy levels serve as the ancilla qubit.

Online content

Any methods, additional references, Nature Research reporting summaries, source data, statements of data availability and associated accession codes are available at https://doi.org/10.1038/s41567-018-0414-3.

Received: 23 May 2018; Accepted: 21 December 2018;
Published online: 11 February 2019

References

1. Nielsen, M. A. & Chuang, I. L. *Quantum Computation And Quantum Information* (Cambridge University Press, Cambridge, 2000).
2. Shor, P. W. Scheme for reducing decoherence in quantum computer memory. *Phys. Rev. A* **52**, 2493–2496 (1995).
3. Steane, A. Multiple particle interference and quantum error correction. *Proc. R. Soc. Lond. A* **452**, 2551–2577 (1996).
4. Gottesman, D. An introduction to quantum error correction and fault-tolerant quantum computation. *Proc. Symp. Appl. Math.* **68**, 13–58 (2010).
5. Fowler, A. G., Mariantoni, M., Martinis, J. M. & Cleland, A. N. Surface codes: towards practical large-scale quantum computation. *Phys. Rev. A* **86**, 032324 (2012).
6. Devoret, M. H. & Schoelkopf, R. J. Superconducting circuits for quantum information: an outlook. *Science* **339**, 1169–1174 (2013).
7. Cory, D. G. et al. Experimental quantum error correction. *Phys. Rev. Lett.* **81**, 2152–2155 (1998).
8. Chiaverini, J. et al. Realization of quantum error correction. *Nature* **432**, 602–605 (2004).
9. Schindler, P. et al. Experimental repetitive quantum error correction. *Science* **332**, 1059–1061 (2011).
10. Reed, M. D. et al. Realization of three-qubit quantum error correction with superconducting circuits. *Nature* **482**, 382–385 (2012).
11. Waldherr, G. et al. Quantum error correction in a solid-state hybrid spin register. *Nature* **506**, 204–207 (2014).
12. Taminiau, T. H., Cramer, J., van der Sar, T., Dobrovitski, V. V. & Hanson, R. Universal control and error correction in multi-qubit spin registers in diamond. *Nat. Nanotechnol.* **9**, 171–176 (2014).
13. Nigg, D. et al. Quantum computations on a topologically encoded qubit. *Science* **345**, 302–305 (2014).
14. Kelly, J. et al. State preservation by repetitive error detection in a superconducting quantum circuit. *Nature* **519**, 66–69 (2015).
15. Corcoles, A. D. et al. Demonstration of a quantum error detection code using a square lattice of four superconducting qubits. *Nat. Commun.* **6**, 6979 (2015).
16. Riste, D. et al. Detecting bit-flip errors in a logical qubit using stabilizer measurements. *Nat. Commun.* **6**, 6983 (2015).
17. Cramer, J. et al. Repeated quantum error correction on a continuously encoded qubit by real-time feedback. *Nat. Commun.* **7**, 11526 (2016).
18. Gottesman, D., Kitaev, A. & Preskill, J. Encoding a qubit in an oscillator. *Phys. Rev. A* **64**, 012310 (2001).
19. Leghtas, Z. et al. Hardware-efficient autonomous quantum memory protection. *Phys. Rev. Lett.* **111**, 120501 (2013).
20. Mirrahimi, M. et al. Dynamically protected cat-qubits: a new paradigm for universal quantum computation. *New J. Phys.* **16**, 045014 (2014).
21. Vlastakis, B. et al. Deterministically encoding quantum information using 100-photon Schrodinger cat states. *Science* **342**, 607–610 (2013).
22. Sun, L. et al. Tracking photon jumps with repeated quantum non-demolition parity measurements. *Nature* **511**, 444–448 (2014).
23. Leghtas, Z. et al. Confining the state of light to a quantum manifold by engineered two-photon loss. *Science* **347**, 853–857 (2015).
24. Ofek, N. et al. Extending the lifetime of a quantum bit with error correction in superconducting circuits. *Nature* **536**, 441–445 (2016).
25. Wang, C. et al. A Schrödinger cat living in two boxes. *Science* **352**, 1087–1091 (2016).
26. Heeres, R. W. et al. Implementing a universal gate set on a logical qubit encoded in an oscillator. *Nat. Commun.* **8**, 94 (2017).
27. Chou, K. S. et al. Deterministic teleportation of a quantum gate between two logical qubits. *Nature* **561**, 368–373 (2018).
28. Rosenblum, S. et al. A CNOT gate between multi-photon qubits encoded in two cavities. *Nat. Commun.* **9**, 652 (2018).
29. Albert, V. V. et al. Performance and structure of single-mode bosonic codes. *Phys. Rev. A* **97**, 032346 (2018).
30. Flühmann, C. et al. Encoding a qubit in a trapped-ion mechanical oscillator. Preprint at https://arxiv.org/abs/1807.01033 (2018).
31. Krastanov, S. et al. Universal control of an oscillator with dispersive coupling to a qubit. *Phys. Rev. A* **92**, 040303 (2015).
32. Michael, M. H. et al. New class of quantum error-correcting codes for a bosonic mode. *Phys. Rev. X* **6**, 031006 (2016).
33. Li, L. et al. Cat codes with optimal decoherence suppression for a lossy bosonic channel. *Phys. Rev. Lett.* **119**, 030502 (2017).
34. Rosenblum, S. et al. Fault-tolerant detection of a quantum error. *Science* **361**, 266–270 (2018).
35. Zhou, S., Zhang, M., Preskill, J. & Jiang, L. Achieving the Heisenberg limit in quantum metrology using quantum error correction. *Nat. Commun.* **9**, 78 (2018).
36. Kurizki, G. et al. Quantum technologies with hybrid systems. *Proc. Natl Acad. Sci. USA* **112**, 3866–3873 (2015).
37. Wallraff, A. et al. Strong coupling of a single photon to a superconducting qubit using circuit quantum electrodynamics. *Nature* **431**, 162–167 (2004).
38. Paik, H. et al. Observation of high coherence in Josephson junction qubits measured in a three-dimensional circuit QED architecture. *Phys. Rev. Lett.* **107**, 240501 (2011).
39. Liu, K. et al. A twofold quantum delayed-choice experiment in a superconducting circuit. *Sci. Adv.* **3**, e1603159 (2017).

40. Kirchmair, G. et al. Observation of quantum state collapse and revival due to the single-photon Kerr effect. *Nature* **495**, 205–209 (2013).
41. Khaneja, N., Reiss, T., Kehlet, C., Schulte-Herbriiggen, T. & Glaser, S. J. Optimal control of coupled spin dynamics: design of NMR pulse sequences by gradient ascent algorithms. *J. Magn. Reson.* **172**, 296–305 (2005).
42. De Fouquieres, P., Schirmer, S., Glaser, S. & Kuprov, I. Second order gradient ascent pulse engineering. *J. Magn. Reson.* **212**, 412–417 (2011).
43. Barends, R. et al. Superconducting quantum circuits at the surface code threshold for fault tolerance. *Nature* **508**, 500–503 (2014).
44. Knill, E. et al. Randomized benchmarking of quantum gates. *Phys. Rev. A* **77**, 012307 (2008).
45. Ryan, C. A., Laforest, M. & Laflamme, R. Randomized benchmarking of single- and multi-qubit control in liquid-state NMR quantum information processing. *New J. Phys.* **11**, 013034 (2009).
46. Magesan, E. et al. Efficient measurement of quantum gate error by interleaved randomized benchmarking. *Phys. Rev. Lett.* **109**, 080505 (2012).
47. Carignan-Dugas, A., Wallman, J. J. & Emerson, J. Characterizing universal gate sets via dihedral benchmarking. *Phys. Rev. A* **92**, 060302 (2015).
48. Cross, A. W., Magesan, E., Bishop, L. S., Smolin, J. A. & Gambetta, J. M. Scalable randomised benchmarking of non-Clifford gates. *npj Quantum Inf.* **2**, 16012 (2016).
49. Harper, R. & Flammia, S. T. Estimating the fidelity of T gates using standard interleaved randomized benchmarking. *Quantum Sci. Technol.* **2**, 015008 (2017).
50. Axline, C. et al. An architecture for integrating planar and 3D cQED devices. *Appl. Phys. Lett.* **109**, 042601 (2016).
51. Chu, Y. et al. Quantum acoustics with superconducting qubits. *Science* **358**, 199–202 (2017).
52. Tabuchi, Y. et al. Coherent coupling between a ferromagnetic magnon and a superconducting qubit. *Science* **349**, 405–408 (2015).
53. Kaufman, A. M., Lester, B. J. & Regal, C. A. Cooling a single atom in an optical tweezer to its quantum ground state. *Phys. Rev. X* **2**, 041014 (2012).
54. Um, M. et al. Phonon arithmetic in a trapped ion system. *Nat. Commun.* **7**, 11410 (2016).

Acknowledgements

We thank N. Ofek and Y. Liu for suggestions on FPGA programming, and L. Jiang, L. Li and R. Schoelkopf for discussions. L.S. acknowledges support from the National Key Research and Development Program of China grant number 2017YFA0304303 and National Natural Science Foundation of China grant number 11474177. S.M.G. acknowledges grants from ARO W911NF1410011 and NSF DMR-1609326. L.S. also thanks R. Vijay and his group for help on the parametric amplifier measurements.

Author contributions

L.H. and L.S. developed the FPGA logic. L.H. and Y.M. performed the experiment and analysed the data with the assistance of W.C., X.M., Y.X. and W.W. L.S. directed the experiment. L.M.D., C.L.Z. and L.S. proposed the experiment. C.-L.Z., Y.W., S.M.G. and L.-M.D. provided theoretical support. W.C. fabricated the JPA. L.H. and X.M. fabricated the devices with the assistance of Y.X., H.W. and Y.P.S. C.-L.Z., S.M.G. and L.S. wrote the manuscript with feedback from all authors.

Competing interests

The authors declare no competing interests.

Additional information

Supplementary information is available for this paper at https://doi.org/10.1038/s41567-018-0414-3.

Reprints and permissions information is available at www.nature.com/reprints.

Correspondence and requests for materials should be addressed to C.-L.Z. or L.S.

Journal peer review information: *Nature Physics* thanks P. van Loock and the other anonymous reviewer(s) for their contribution to the peer review of this work.

Publisher's note: Springer Nature remains neutral with regard to jurisdictional claims in published maps and institutional affiliations.

© The Author(s), under exclusive licence to Springer Nature Limited 2019

Methods

The ancillary transmon qubit has a frequency $\omega_q/2\pi = 5.692$ GHz, an energy relaxation time $T_1 = 30$ µs, and a pure phasing time $T_\phi = 120$ µs. The binomial code is encoded in the storage cavity (the oscillator) with a frequency $\omega_s/2\pi = 7.634$ GHz, a single-photon lifetime $\tau_s = 143$ µs ($\kappa_s/2\pi = 1.1$ kHz), and a coherence time 252 µs. The self-Kerr of the oscillator induced by the ancilla qubit is $K_s/2\pi = 4.2$ kHz. The logical qubit can be manipulated by the ancillary qubit through its dispersive interaction with the oscillator, $\chi_{qs}/2\pi = 1.90$ MHz. The readout cavity is at a frequency of $\omega_r/2\pi = 8.610$ GHz and has a lifetime of 44 ns, such that $\kappa_r/2\pi = 3.62$ MHz is matched with the dispersive interaction between the ancilla qubit and the readout cavity $\chi_{qr}/2\pi = 3.65$ MHz for a best readout signal-to-noise ratio. A Josephson parametric amplifier is also used for a high-fidelity and high-QND single-shot readout of the ancilla qubit with a duration of 320 ns: >99.9% for the ground state $|g\rangle$ and 98.9% for the excited state $|e\rangle$. The dispersive interaction allows for a Ramsey-type parity measurement of the photon numbers in the oscillator, where two unconditional $\pi/2$ rotations of the ancilla qubit are separated by a delay of $\pi/\chi_{qs} \approx 260$ ns, with >99.9% QND and a fidelity of 97.2% for $\bar{n} = 2$. An error syndrome measurement process takes about 1 µs, during which a photon loss occurs with a possibility of 1.4%.

The ancilla qubit, the oscillator and the readout cavity are each controlled by a field programmable gate array with home-made logic, allowing for both a fast readout of the ancilla qubit and a fast real-time feedback control of the oscillator with a latency of about 330 ns (the time interval between sending out the last point of the readout signal and sending out the first point of the control signal) including the signal travel time through the experimental circuitry, which is about 1% of the ancilla qubit lifetime.

Process tomography is realized by preparing four linear independent initial states $\{|g\rangle, |e\rangle, (|g\rangle + |e\rangle)/\sqrt{2}, (|g\rangle - i\,|e\rangle/\sqrt{2})\}$, and then performing the corresponding final-state tomography of the ancilla after encoding, repetitive QEC and decoding information back to the ancilla. From these processes, we derive the 4×4 process matrix χ_M. The fidelity is defined as the overlap between χ_M and χ_I (χ_I is for a perfect QEC process) $F_\chi = \mathrm{tr}(\chi_M\chi_I)$.

Supplementary methods. For more details, including those regarding the experimental device and set-up, comparison between binomial codes and cat codes, measured system parameters, coherence times, measurement properties, experimental sequences, T gate fidelity, and theoretical analysis and error model of QEC performance, see the Supplementary Information.

Data availability

The data that support the plots within this paper and other findings of this study are available from the corresponding authors upon request.